

Improvement in Labeling Efficiency of Hydrophilic and Hydrophobic Fluorescent Molecules in Thick Tissue Sections

Po-Hang Tseng,¹ Shu-Jen Chiang,¹ Shean-Jen Chen,^{2#} and Chen-Yuan Dong^{1*}

¹Department of Physics, National Taiwan University, Taipei 106, Taiwan, Republic of China

²Institute of Photonics, National Chiao-Tung University, Tainan 711, Taiwan, Republic of China

#sheanjen@nctu.edu.tw, *cydong@phys.ntu.edu.tw

Abstract: In this work, we investigated the labeling efficiency of hydrophilic (DAPI) and hydrophobic (Nile Red) fluorescent probes using uni- and bi-directional diffusion on porcine liver tissue sections on the order of a few hundred microns in thickness. Bi-directional diffusion significantly enhanced the penetration of probes. Although diffusion most accurately describes the labeling process, we found that after removal of the labeling molecules residual probe molecules in the tissue sections continued to be transported deeper into the tissue resulting in additional tissue constituents being labeled. Our study shows that bi-directional labeling can significantly enhance the labeling of thick tissues for applications in which structural information in three dimensions is needed.

Keywords: multiphoton microscopy, tissue sections, diffusion, labeling enhancement, liver

Introduction

In recent years, significant research efforts in biomedical imaging have focused on obtaining three-dimensional morphological and molecular structure at the whole-organ level. In connectome research, this approach has clear significance in that connections among neurons are critically related to neurological function [1–3]. Medically, mapping immune biomarkers in three dimensions may lead to identification of patients who best respond to immune checkpoint inhibitor therapy (ICIT) [4–6]. Several tissue clearing techniques have been developed for biomedical imaging in three dimensions. An example is X-CLARITY™ (Logos Biosystems), which optically clears tissues for subsequent fluorescence labeling of thick tissues or, in some cases, entire organs of interest [7–9]. Combined with light-sheet microscopy, structural mapping of an entire animal mouse brain has been achieved. Although optical clearing techniques enable whole-organ labeling and imaging, these methods suffer from numerous disadvantages such as prolonged tissue clearing and labeling times and compromised structural resolution from the use of microscope objectives with relatively small numerical apertures [10,11]. To address these issues, another paradigm is to section the organ of interest to obtain thin tissue slices for further processing such as optical clearing and labeling [8,10,11], however, this is a time-consuming process and reduces efficiency when reconstructing an organ in three dimensions.

In the case of diffusion, the effective label penetration depth is proportional to the square of the labeling time. Specifically, the one-dimensional diffusion process is described by the equation:

$$\langle x^2 \rangle = 2Dt \quad (1)$$

where $\langle x^2 \rangle$ is the average of the square of probe penetration depth, D is the molecular diffusion constant, and t is the diffusion time [12]. Therefore, processing the organ of interest into thin sections prior to labeling significantly increases labeling efficiency. For example, diffusion across a 100 μm tissue section takes 10^{-4} the time that is required for a probe molecule to penetrate a 1 cm organ. Nevertheless, antibody labeling of a thin tissue section can still be time-consuming, and currently the standard approach is to leave the tissue section in the labeling solution in a trial-and-error fashion to find the optimal labeling conditions.

To enhance the labeling efficiency of tissue sections, we developed a bi-directional labeling device to compare the labeling efficiency on porcine liver slices to the standard uni-directional labeling approach. Diffusion of two commonly used probe molecules with distinct chemical properties was studied: DAPI, a hydrophilic DNA dye commonly used for nuclear labeling, and Nile Red, a lipophilic membrane probe.

Materials and Methods

Figure 1 illustrates the sample preparation steps. Porcine liver acquired from a local market was cut into approximately 1 cm thick sections and fixed in 10% formalin (Avantor, Inc., Radnor, PA) at room temperature for approximately 24 hr. After fixation, the tissues were placed in phosphate buffered saline (PBS) and kept under refrigeration. Three-millimeter cylindrical punches of tissue were obtained with a Uni-Core™ punch (GE Healthcare Bio-Sciences Corp., Piscataway, NJ). The 3 mm tissue core was placed upright and surrounded by an acrylic holder 1 cm in diameter. Molten 2% agarose gel (A0576-100G, Sigma-Aldrich, St. Louis, MO) at 40–45°C was then dripped onto the tissue core and cooled under refrigeration for 30 min. The agarose embedded tissue core was then placed in a 1.6 cm diameter stainless steel holder designed for sectioning with a vibrating blade microtome (Compressome®, Precisionary Instruments, Natick, MA). To obtain porcine liver sections, the Compressome® sectioning thickness was set to 250 μm , and the agarose embedded tissue was sectioned while immersed in deionized water at 4°C. Upon sectioning, the tissue slice was immediately removed and placed in PBS at room temperature.

For uni-directional diffusion labeling (Figure 2(a)), a single well of a 48-well plate (SPL Life Sciences Co., Ltd., Pocheon, Korea) was filled with 1 ml PBS buffer, and the tissue section was then placed into the well. After the tissue section sank to the bottom of the well, the PBS was pipetted out and the

i-PRO

The Power of Truth

WHEN PRECISION AND ACCURACY MATTER MOST

Panasonic i-PRO Sensing Solutions imaging devices deliver the extreme accuracy only available with ultra-HD technology. Our products feature high-resolution imaging, high-color reproduction, high sensitivity and are compact sized. Our micro-head cameras are used in the most sophisticated scopes and diagnostic devices with consistent results and reliability.

Visit our website to learn more:
medicalimaging.i-pro.com



Panasonic

An Imaging Solution Provider

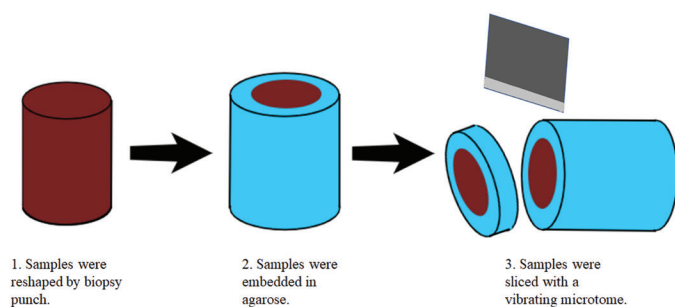


Figure 1: Porcine liver tissue handling process.

labeling solution introduced to the well. In the bi-directional labeling geometry (Figure 2(b)), the tissue slice was positioned within a custom-made labeling chamber in which the liver section was sandwiched between the upper and bottom chambers, both filled with the labeling solution. For tissue labeling, 40 μM of DAPI (MW 350.3, Invitrogen, Carlsbad, CA) and 100 μM of Nile Red (MW 318.4, Sigma-Aldrich) were used. In all, six incubation periods of 5 min, 45 min, 130 min, 215 min, 12 hr, and 24 hr were applied to the liver sections. Incubation was performed under room temperature, and staining wells were held stationary and protected from light. The similar molecular weights of DAPI and Nile Red indicate that they have similar diffusion properties. At the end of the scheduled incubation period, the tissue slices were removed, washed with PBS, and imaged with a homemade multiphoton microscope (described below). To visualize the dye distribution, the stained liver sections were cut vertically to expose the dye distribution across the tissue cross sections. For each tissue section, three random sites were analyzed to determine mean staining depth and standard deviation.

At the end of the incubation period, a time window was needed to process the tissue section for multiphoton imaging, therefore an additional tissue processing time constant t_p was applied to Equation (1). During t_p , remnant probe molecules in the tissue slices can diffuse and interact further with the tissue

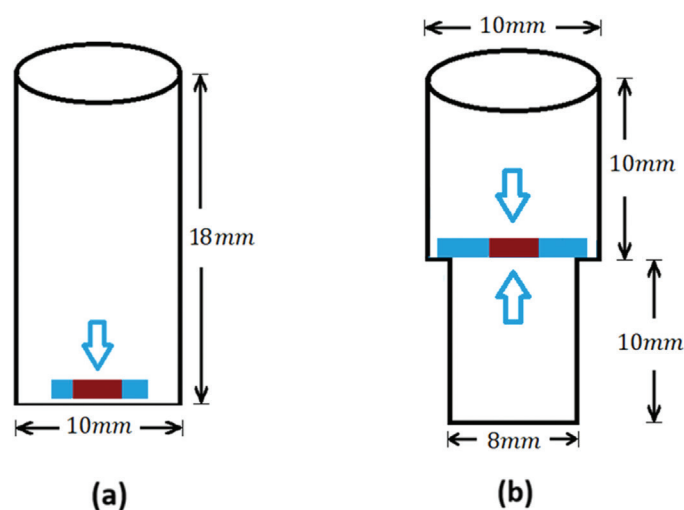


Figure 2: (a) Uni-directional tissue slice labeling chamber and (b) bi-directional tissue labeling chamber geometry. Brown represents the tissue section surrounded by blue agarose. Blue arrows represent directions of dye diffusion.

constituents, resulting in greater dye penetration depth than that predicted by Equation (1). As a result, Equation (1) was modified to include the effect of t_p (Equation (2))

$$\langle x^2 \rangle = 2D(t + t_p). \quad (2)$$

A comparison of Equations (1) and (2) shows that t_p is simply the x-intercept of a plot of $\langle x^2 \rangle$ as a function of t (Equation (1)).

Our imaging system consists of an inverted microscope (TE2000U, Nikon, Japan) with a titanium-sapphire (Ti:Sapph) diode-pumped laser (Tsunami[®], Spectra Physics, Santa Clara, CA) and a solid-state laser operating at 532 nm (Millennia[®] Pro, Spectra Physics). The 780 nm output of the Ti:Sapph laser was used as the excitation source. Upon reflection from a galvanometer-driven x-y scanning system (6215M, Cambridge Technology, Watertown, MA), the laser was beam-expanded and reflected into the focusing objective (S Fluor, 20 \times /NA 0.75, Nikon) by a primary dichroic mirror (720 dcspxr, Chroma Technology, Bellows Falls, VT). Laser power at the sample was approximately 40–50 mW for DAPI-stained samples and 20 mW for Nile Red-labeled specimens. We used blue fluorescence for detecting DAPI and red fluorescence for Nile Red. Single-photon counting photomultipliers (R7400P, Hamamatsu, Hamamatsu City, Japan) were used to detect emitted photons.

Results and Discussion

Cross-sectional fluorescence intensity distribution patterns of DAPI and Nile Red at different timepoints under uni- and bi-directional diffusion are shown in Figure 3. Qualitatively, with increased incubation time, the dye molecules penetrated deeper into the tissue section. Moreover, it is evident that dye penetration is more efficient in the bi-directional geometry. Specifically, at 215 min, DAPI has nearly penetrated the entire tissue slice, whereas uni-directional diffusion of DAPI across the tissue section was not noticed until 24 hr after incubation. On the other hand, while Nile Red penetration is nearly complete at the 215-minute timepoint for both incubation geometries, earlier timepoints show greater efficiency in Nile Red labeling. Since DAPI and Nile Red have similar MW (~300), the difference in diffusion efficiency between the two types of molecules is most likely due to Nile Red targeting cellular membranes. Since hepatocytes are tightly packed, the close proximity of plasma membranes of adjacent hepatocytes may favor the diffusion of Nile Red over DAPI.

Next, we plotted representative normalized probe fluorescence distribution profiles for DAPI (Figure 4) and Nile Red (Figure 5) for both uni- and bi-directional labeling geometries at the selected timepoints of 130 min and 24 hr. With uni-directional labeling in which the tissue section is in contact with the bottom of the labeling chamber, diffusion efficiency is significantly hindered, as only 30% or less of the intensity is registered at the bottom of the section when compared to the top. Differences in labeling efficiency between the top and bottom decreased with increased incubation time. Although a fluorescence intensity gradient was observed for DAPI (Figure 4), the Nile Red profiles (Figure 5) demonstrated similar labeling efficiency between the top and bottom of the section. To further quantify the efficiencies of the labeling geometries for the two chemically distinct

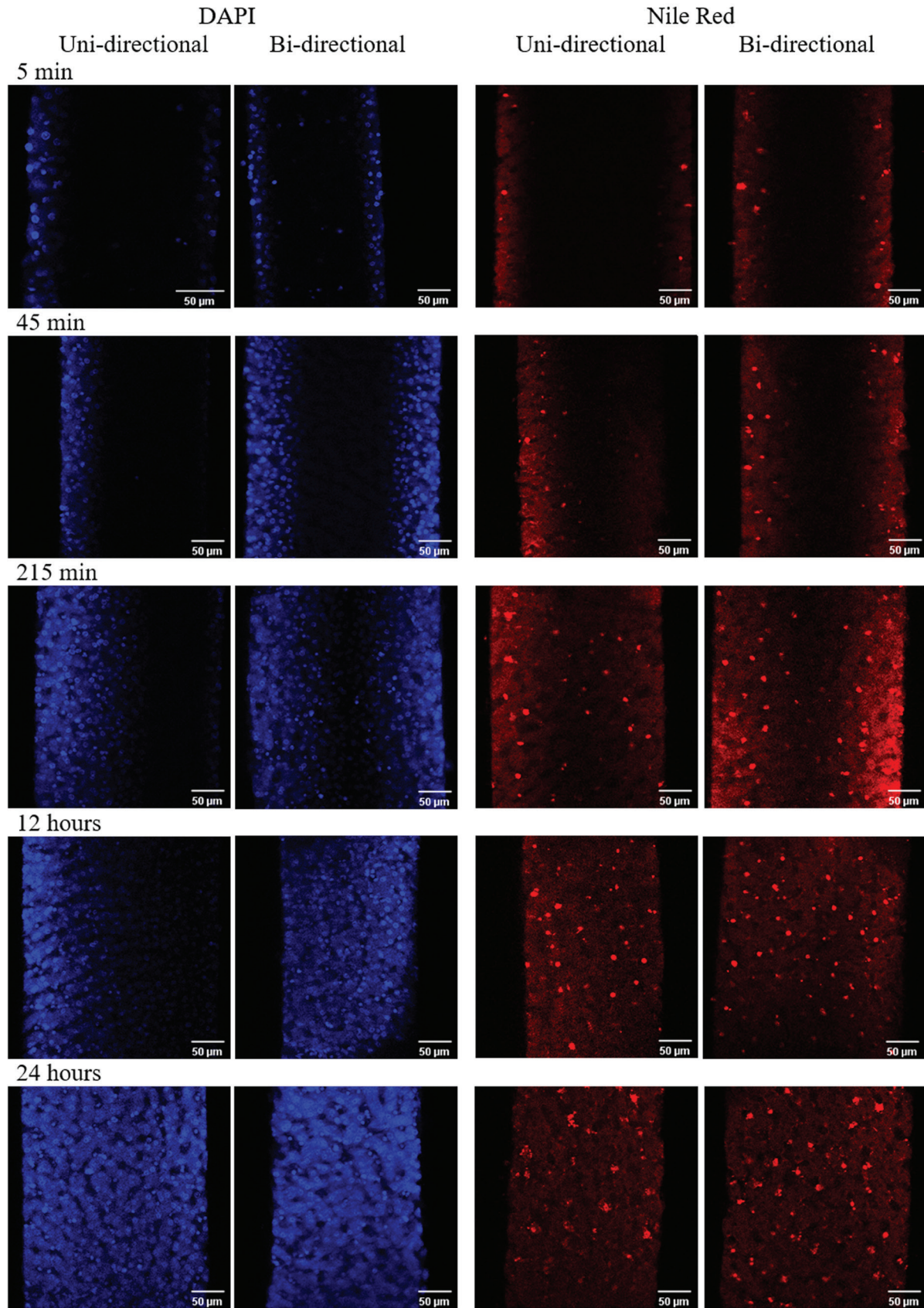


Figure 3: Time-lapse imaging of cross sections of DAPI- or Nile Red-labeled porcine liver slices by uni-directional and bi-directional diffusion. Each row of four images represents a labeling time noted above the row. Notice that with bi-directional diffusion, labels penetrate the tissue faster.

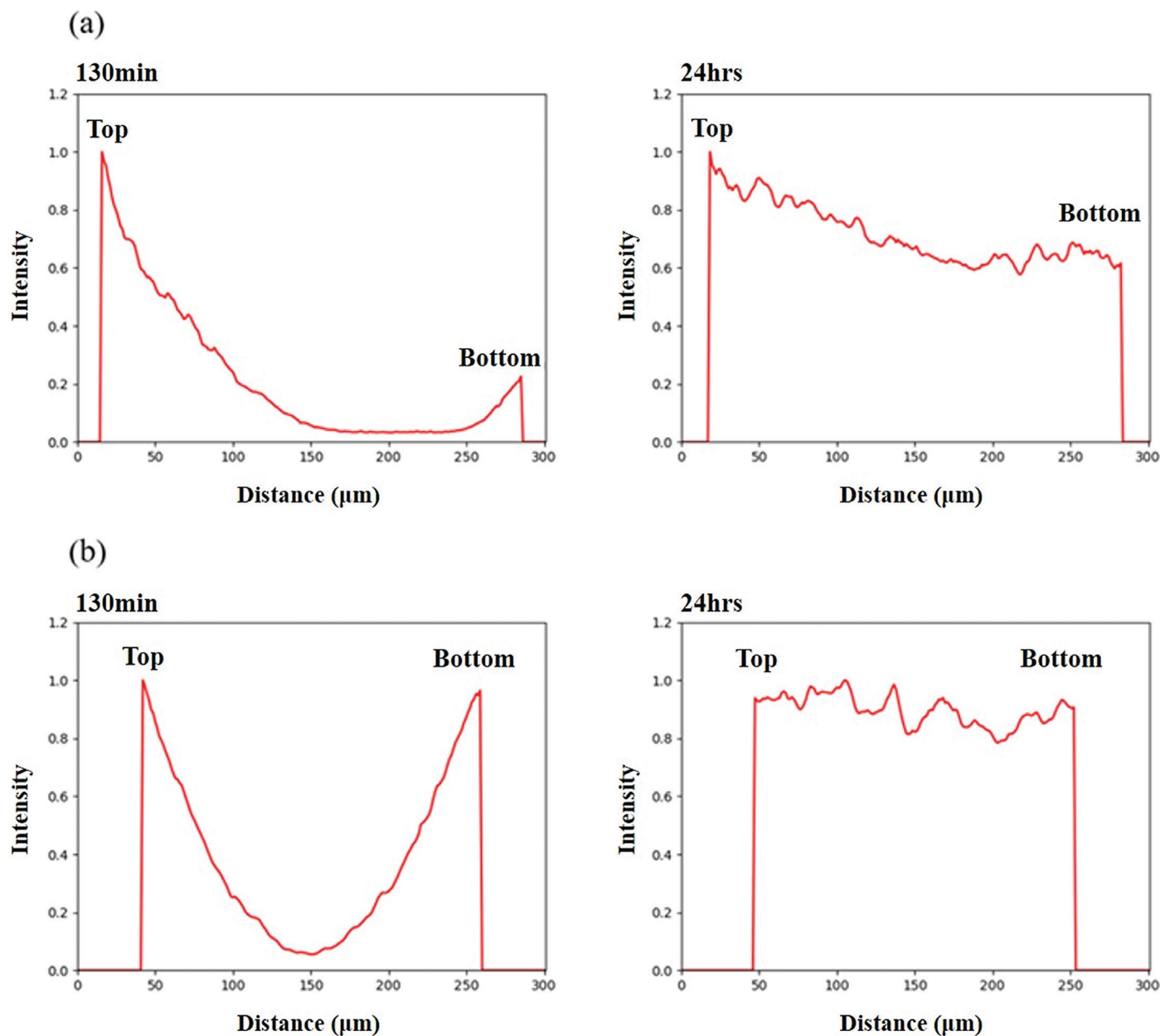


Figure 4: Time-dependent fluorescence intensity profiles of DAPI through (a) uni- and (b) bi-directional diffusion. Top and bottom refer to the two surfaces of the tissue section.

probe molecules, we estimated the effective diffusion distance as a function of time. For DAPI-labeled samples, we computed the effective diffusion distance from both the top and bottom surfaces to where the probe fluorescence intensity was decreased to a threshold defined as 10% of the peak value at the respective surfaces. For Nile Red, this threshold was set to 20% of the peak value. The choice of selecting different threshold values for DAPI and Nile Red was motivated by the observation that Nile Red penetrated faster than DAPI, and we wanted to analyze diffusion at similar depths in the tissue for a given labeling time such that the relative diffusion efficiency of the two dyes could be compared. This was performed as if probe molecules had diffused from the top and bottom sides and had not reached the same position within the tissue. Hence, estimation of diffusion length

using Equation 1 is justified. The results for DAPI and Nile Red are shown in Tables 1 and 2, respectively.

By defining x_{rms} as the root mean square of position x , we plotted the x_{rms}^2 ($\langle x^2 \rangle$) as a function of time for the top surface of the uni-directional geometry and for the average of the top and bottom surfaces of the bi-directional geometry in Figure 6. The linearity of the plots shows that Equation (1) is a good model for describing molecular transport in our diffusion geometries. Additionally, note that in each case the tissue processing and imaging time constant t_p was needed. For a set of diffusion data with four different labeling times (t): 5 min, 45 min, 130 min, and 215 min, the graph of x_{rms}^2 as a function of t are shown in Figure 6. By applying a linear fit (Equation (2)), we found that t_p varied between 9.4 and 30.1 min.

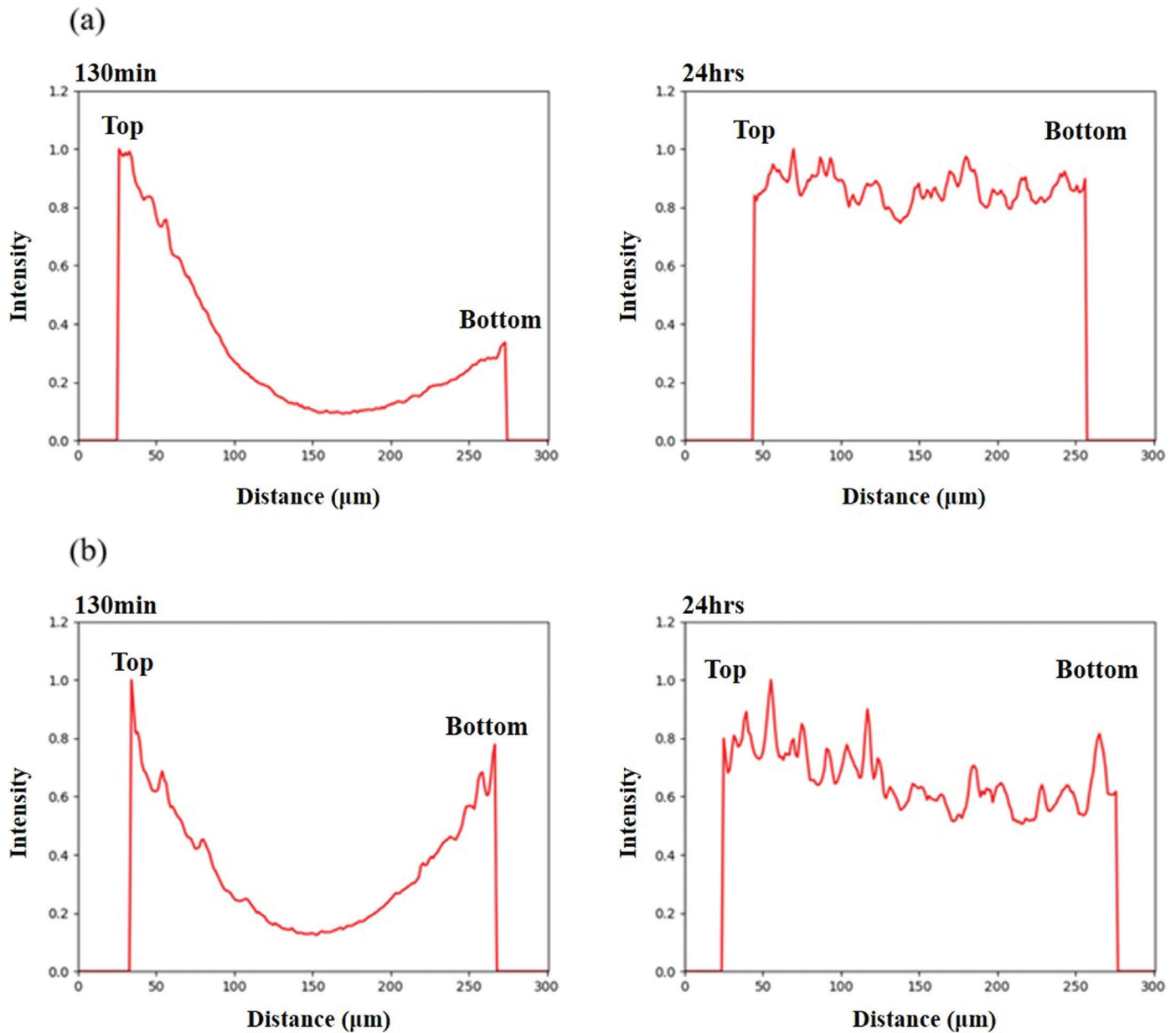


Figure 5: Time-dependent fluorescence intensity profiles of Nile Red through (a) uni- and (b) bi-directional diffusion. Top and bottom refer to the two surfaces of the tissue section.

Conclusions

In this work, we investigated the labeling efficiency of hydrophilic DAPI and hydrophobic Nile Red fluorescent probes in porcine liver slices. Multiphoton imaging was

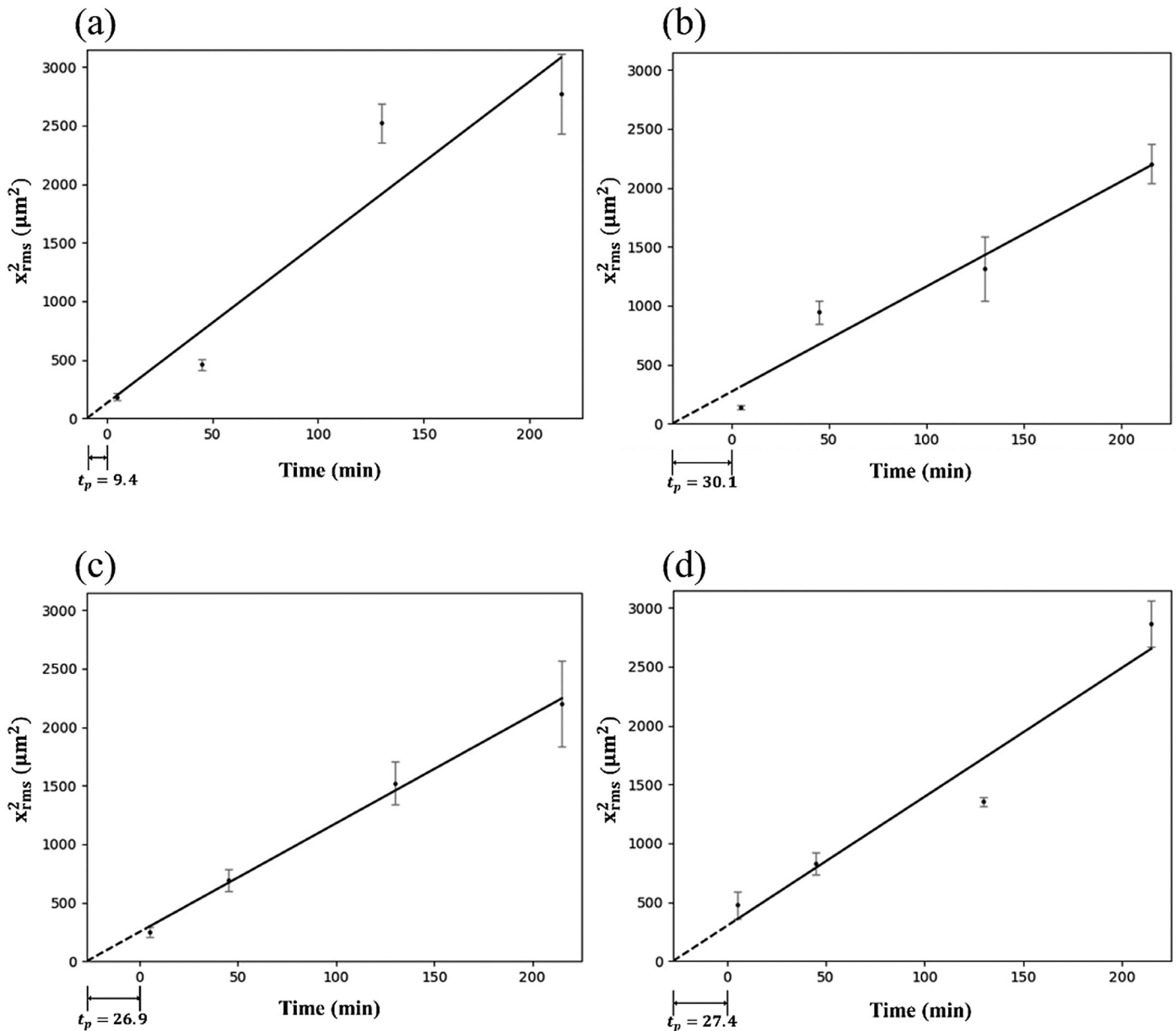
performed on cross sections of the slices after diffusion by uni- and bi-directional geometries. We found that bi-directional diffusion significantly enhanced the penetration of probe diffusion efficiency and that diffusion most accurately describes

Table 1. Uni- and bi-directional diffusion of DAPI.

Time	Uni-directional		Bi-directional	
	Top x_{rms} (μm)	Bottom x_{rms} (μm)	Top x_{rms} (μm)	Bottom x_{rms} (μm)
5 min	10.9 ± 0.4	8.5 ± 0.7	11.7 ± 0.6	0.2 ± 0.4
45 min	27.1 ± 1.6	28.0 ± 0.5	18.5 ± 1.1	0.0 ± 0.0
130 min	29.9 ± 4.2	31.8 ± 3.2	42.0 ± 1.9	2.1 ± 1.8
215 min	42.6 ± 1.9	34.9 ± 3.3	45.9 ± 2.2	0.0 ± 0.0

Table 2. Uni- and bi-directional diffusion of Nile Red.

Time	Uni-directional		Bi-directional	
	Top x_{rms} (μm)	Bottom x_{rms} (μm)	Top x_{rms} (μm)	Bottom x_{rms} (μm)
5 min	15.8 \pm 1.3	11.9 \pm 1.1	22.5 \pm 3.3	20.9 \pm 2.0
45 min	26.3 \pm 1.8	19.8 \pm 6.6	29.5 \pm 2.0	27.9 \pm 1.1
130 min	39.0 \pm 2.4	16.8 \pm 5.9	36.8 \pm 0.5	36.8 \pm 0.5
215 min	46.8 \pm 4.0	34.6 \pm 3.2	53.8 \pm 1.7	53.2 \pm 2.0

**Figure 6:** Plot of x_{rms}^2 as a function of time with (a) DAPI uni-directional diffusion, (b) DAPI bi-directional diffusion, (c) Nile Red uni-directional diffusion, and (d) Nile Red bi-directional diffusion.

the labeling process. However, we found that after removal of the tissue slices from the labeling solutions, residual probe molecules in the tissue sections continue to be transported resulting in the labeling of additional tissue constituents. Our

study supports the use of bi-directional labeling for enhanced efficiency in the labeling of thick tissues for applications in connectome and other biomedical topics in which structural information in three dimensions is needed.

Acknowledgement

This work was supported by the Ministry of Science and Technology, Taiwan, Republic of China (MOST 107-2112-M-002-023-MY3).

References

- [1] K Amunts et al., *Science* 340 (2013) doi.org/10.1126/science.1235381.
- [2] M Helmstaedter et al., *Nature* 514 (2014) doi.org/10.1038/nature13877.
- [3] CS Xu, et al., *bioRxiv* (2020) doi.org/10.1101/2020.01.21.911859.
- [4] JR Brahmer et al., *J Clin Oncol* 36 (2018) doi.org/10.1200/JCO.2017.77.6385.
- [5] JR Lin et al., *eLife* 7 (2018) doi.org/10.7554/eLife.31657.
- [6] T Tsujikawa et al., *Cell Reports* 19 (2017) doi.org/10.1016/j.celrep.2017.03.037.
- [7] SY Kim et al., *Proc Natl Acad Sci USA* 112 (2015) doi.org/10.1073/pnas.1510133112.
- [8] X Zhu et al., *Proc Natl Acad Sci USA* 116 (2019) doi.org/10.1073/pnas.1819583116.
- [9] IP Pavlova et al., *Hippocampus* 28 (2018) doi.org/10.1002/hipo.22951.
- [10] SSY Lee et al., *Sci Rep* 7 (2017) doi.org/10.1038/s41598-017-16987-x.
- [11] M Morawski et al., *NeuroImage* 182 (2018) doi.org/10.1016/j.neuroimage.2017.11.060.
- [12] X Bian et al., *Soft Matter* 12 (2016) doi.org/10.1039/C6SM01153E.

MT



Salamander Epidermis Glia - Louise Lewis
Bioscience Electron Microscopy Lab, University of Connecticut



931 GL
tousimis
tousimis research corporation



Fractal Nanotrus
CalTech, Materials Science and Mechanics (Julia R. Greer & Green Group)

Advanced Multi Application Programmable Critical Point Dryer



tousimis

Autosamdri®-931

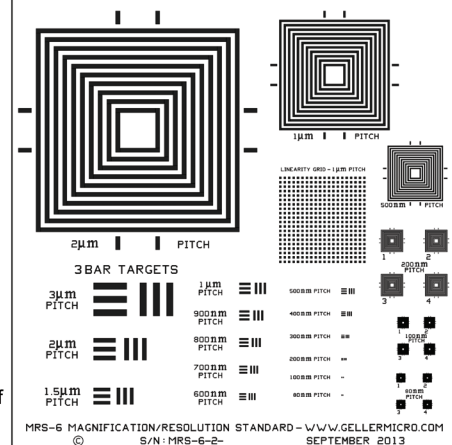
tousimis.com

MRS-6


We are ISO-9000 certified and ISO-17025 accredited
Microscopy Calibration Standard

Now you can calibrate better from 1,000X to 1,000,000X!

This is our fifth generation, traceable, magnification reference standard for all types (SEM, FESEM, Optical, STM, AFM, etc.) of microscopy. The MRS-6 has multiple X and Y pitch patterns ranging from 80nm (± 3 nm) to 2 μ m and 3 bar targets from 80nm to 3 μ m. There is also a STM test pattern. Definition of the 80 nm pitch pattern is excellent.



MRS-6 MAGNIFICATION/RESOLUTION STANDARD - WWW.GELLERMICRO.COM
© S/N: MRS-6-2- SEPTEMBER 2013



GELLER MICROANALYTICAL LABORATORY, Inc.

426e BOSTON ST., TOPSFIELD, MA 01983-1216
TEL: 978 887-7000 FAX: 978-887-6671
www.GellerMicro.com